PET imaging of hypoxia-inducible factor-1-active tumor cells with pretargeted oxygen-dependent degradable streptavidin and a novel [18]F-labeled biotin derivative.

AUTHOR(S):

Kudo, Takashi; Ueda, Masashi; Konishi, Hiroaki; Kawashima, Hidekazu; Kuge, Yuji; Mukai, Takahiro; Miyano, Azusa; ... Kizaka-Kondoh, Shinae; Hiraoka, Masahiro; Saji, Hideo

CITATION:

Kudo, Takashi ...[et al]. PET imaging of hypoxia-inducible factor-1-active tumor cells with pretargeted oxygen-dependent degradable streptavidin and a novel [18]F-labeled biotin derivative.. Molecular imaging and biology 2011, 13(5): 1003-1010

ISSUE DATE:

2011-10

URL:

http://hdl.handle.net/2433/153020

Title Page:

PET imaging of hypoxia-inducible factor-1-active tumor cells with pretargeted oxygen-dependent degradable streptavidin and a novel ^{18}F-labeled-biotin derivative

Takashi Kudo[1], Masashi Ueda[1,2], Hiroaki Konishi[1], Hidekazu Kawashima[1,3], Yuji Kuge[1,4], Takahiro Mukai[5], Azusa Miyano[1], Shotaro Tanaka[6], Shinae Kizaka-Kondoh[6], Masahiro Hiraoka[6], Hideo Saji[1]

[1]Department of Patho-Functional Bioanalysis, Graduate School of Pharmaceutical Sciences, Kyoto University, Kyoto 606-8501, Japan

[2]Radioisotopes Research Laboratory, Kyoto University Hospital, Faculty of Medicine, Kyoto University, Kyoto 606-8507, Japan

[3]Department of Nuclear Medicine and Diagnostic Imaging, Graduate School of Medicine, Kyoto University, Kyoto 606-8507, Japan

[4]Central Institute of Isotope Science, Hokkaido University, Sapporo 060-0815, Japan

[5]Department of Biomolecular Recognition Chemistry, Graduate School of Pharmaceutical Sciences, Kyushu University, Fukuoka 812-8582, Japan

[6]Department of Radiation Oncology and Image-applied Therapy, Graduate School of Medicine, Kyoto University, Kyoto 606-8507, Japan

Corresponding author:

Hideo Saji, PhD

Department of Patho-Functional Bioanalysis

Graduate School of Pharmaceutical Sciences

Kyoto University

46-29 Yoshida Shimoadachi-cho, Sakyo-ku, Kyoto 606-8501, Japan.

E-mail address: hsaji@pharm.kyoto-u.ac.jp

Phone: (+81/0) 75-753-4556, Fax: (+81/0) 75-753-4568

Running Title:

PET imaging for HIF-1-active tumors

Manuscript category:

Article

Abstract

Purpose

We aimed to evaluate the feasibility of using streptavidin–biotin-based pretargeting for positron emission tomography (PET) imaging of hypoxia-inducible factor (HIF)-1-active tumors.

Procedures

We used POS, a genetically engineered form of streptavidin that selectively stabilizes in HIF-1-active cells, and (4-^{18}F-fluorobenzoyl)norbiotinamide (^{18}F-FBB), a radiolabelled biotin derivative, for performing a biodistribution study and for PET imaging. The tumoral ^{18}F-FBB accumulation was compared to the HIF-1-dependent luciferase bioluminescence and HIF-1α immunohistochemical signal.

Results

^{18}F-FBB accumulation was observed in POS-pretargeted tumors in mice (2.85% ± 0.55% injected dose/g at 3h), and clear PET images were obtained at the same time point. The tumoral ^{18}F-FBB accumulation positively correlated with luciferase bioluminescence ($R = 0.72$, $P < 0.05$), and most of the area showing ^{18}F-FBB accumulation corresponded to HIF-1α-positive areas.

Conclusion

Pretargeting with POS and ^{18}F-FBB is an effective approach for PET imaging of HIF-1-active areas in tumors.

Key Words

Tumor hypoxia; Hypoxia-inducible Factor-1 (HIF-1); Oxygen-dependent degradation domain (ODD); Pretargeting; ^{18}F-labeled biotin derivative

Introduction

Abnormal rapid growth of tumor cells outstrips the blood supply, which develops an oxygen tension below physiologic levels (hypoxia) [1]. It appears to be strongly associated with malignant progression and the development of radioresistance [2, 3]. The transcription factor hypoxia-inducible factor-1 (HIF-1) has been reported to be one of the critical components of hypoxic responses [4]. Because HIF-1 was recently reported to be closely related to tumor malignancy and to hinder both chemotherapy and radiation therapy [5, 6], noninvasive imaging of HIF-1-active hypoxic tumor cells may be useful in making a qualitative diagnosis and establishing a therapy for cancer. The oxygen-sensitive alpha subunit of HIF-1 (HIF-1α) contains an oxygen-dependent degradation domain (ODD) and regulates the HIF-1 activity by inducing the degradation of HIF-1 via the ODD under normoxic conditions [7]. Therefore, it is likely that a probe that contains the ODD and induces degradation in a similar manner as HIF-1α does can be used to evaluate HIF-1 activity *in vivo*.

We have recently synthesized proteins in which the protein transduction domain (PTD) is fused to the ODD and demonstrated that these proteins were efficiently delivered to hypoxic regions and were stabilized in HIF-1-active cells [8-11]. We have also fused the PTD and the ODD with a monomeric streptavidin (SAV) to produce a chimeric protein, PTD-ODD-SAV (POS), and synthesized a radiolabelled biotin derivative, (3-$^{123/125}$Iiodobenzoyl)norbiotinamide ($^{123/125}$I-IBB). POS was degraded in an

oxygen-dependent manner, and a clear image of the tumor was obtained at 24 h after the injection of ^{123}I-IBB-conjugated-POS of which accumulation in the tumor was found to correlate with the HIF-1 activity [12]. Furthermore, we were able to obtain the tumor image rapidly by using of a pretargeting approach. The adequate-contrast image was obtained just 6 h after injection of ^{123}I-IBB in the pretargeting approach, while 24 h was required in the case using ^{123}I-IBB-conjugated-POS [13].

Compared to single-photon emission computed tomography imaging, positron emission tomography (PET) imaging is more sensitive and more quantitative, and provides images with higher spatial resolution. The limited and heterogenous expression of HIF-1 in the tumor required a high-spatial-resolution device for the accurate imaging of HIF-1-expressed regions. Therefore, we attempted to obtain PET images of the HIF-1-active hypoxic tumors by using POS. Since it required 24 h to obtain the adequate image using directly-radiolabeled POS [12], we adopted the prertargeting approach to reduce radiation exposure.

Fluorine-18 is one of the most widely used positron emitters because of its adequate half-life, ease of production, and low positron energy; hence, a ^{18}F-labeled biotin derivative may be useful in PET imaging. However, there have been few reports of the application of such a molecule in pretargeted imaging [14]. Therefore, we synthesized (4-^{18}F-fluorobenzoyl)norbiotinamide (^{18}F-FBB) in order to perform PET studies with POS. This study aimed to evaluate the feasibility of using POS and ^{18}F-FBB for pretargeted PET

imaging of HIF-1-active areas in tumors.

Materials and Methods

Synthesis of $^{18/19}$F-FBB

N-Succinimidyl-4-fluorobenzoate (SFB, compound **2**) was synthesized according to a previously described method [15]. The detailed method of FBB (compound **3**) synthesis has been described in the supplemental materials.

The synthesis of ^{18}F-FBB (^{18}F-**3**) is outlined in Fig. 1. Fluorine-18 was produced via the ^{18}O(p,n)^{18}F nuclear reaction by using a proton beam current to irradiate ^{18}O-H_2O [16, 17]. ^{18}F-SFB (^{18}F-**2**) was synthesized according to a previously described method [18, 19] and obtained with decay-uncorrected radiochemical yield of 30–40%. ^{18}F-SFB was then concentrated under a stream of nitrogen and added to a solution of *N,N'*-dimethylformamide (DMF):water (4:1); the DMF solution contained norbiotinamine hydrochloride (5 mg/mL). NEt_3 was added to make the solution basic. The reaction was performed at room temperature for 0.5–1 h, and the reaction mixture was loaded onto a C18 Sep-Pak cartridge (Waters, Milford, MA). The C18 cartridge was eluted with water and then with acetonitrile. The acetonitrile fraction was evaporated, and the residue was purified using high-performance liquid chromatography (HPLC) (Cosmosil 5C_{18}MS-II column; Nacalai Tesque, Kyoto, Japan; 25% acetonitrile; flow rate, 1 mL/min). The retention time of ^{18}F-FBB was 11 min. The

radiochemical purity was measured using HPLC, and the specific activity was determined on the basis of the ultraviolet (UV) absorbance at 254 nm. The solvent was removed by rotary evaporation and reconstituted in water or saline for use in *in vitro* and *in vivo* studies.

Preparation of fusion protein

POS was overexpressed in *Escherichia coli* and purified as described in a previous report [12]. Purified POS was dissolved in Tris-HCl buffer (pH 8.0).

Binding of POS and ^{18}F-FBB

^{18}F-FBB, D-biotin (0–500 pmol), and POS (0.04 pmol) were mixed and incubated in 100 mM citrate buffer (pH 5.0) for 1 h at 37°C. The binding of ^{18}F-FBB to POS in the absence of D-biotin was detected using size-exclusion chromatography (PD-10; GE Healthcare Bioscience, Uppsala, Sweden). The reaction mixture containing D-biotin was applied to an Amicon Microcon filter (Millipore) and centrifuged at 4500 × *g* for 30 min at 4°C (Micro Cooling Centrifuge 1720; Kubota, Osaka, Japan). The radioactivities of the reactant and filtrate (unbound ^{18}F-FBB) were measured, and the binding rate was calculated. All measurements were performed in triplicate.

Cell and cell culture

FM3A mouse mammary tumor cells were purchased from Health Science Research

Resources Bank (Osaka, Japan). Suit2 human pancreatic tumor cells were originally obtained from American Type Culture Collection (Manassas, VA). Suit2/5HRE-CMV$_{mp}$-Luciferase (Suit2/Luc) cells that express luciferase in response to HIF-1 activity were established and supplied by Prof. Kizaka-Kondoh [20]. Both the cell types were cultured using a previously reported method [12, 13].

Animal model

Animal studies were conducted in accordance with our institutional guidelines, and the experimental procedures were approved by the Kyoto University Animal Care Committee. Female C3H/He mice and BALB/c *nu*/*nu* mice at 5 weeks of age were purchased from Japan SLC, Inc. (Hamamatsu, Japan). Models of FM3A and Suit2/Luc tumors were prepared as described in a previous report [12]. After tumor implantation, mice were fed an AIN76-A-based, biotin-free diet (Oriental Yeast Co. Ltd., Tokyo, Japan) in order to prevent dietary biotin from inhibiting the binding of ^{18}F-FBB to POS. The mice were subjected to a tracer study at 2–3 weeks after the implantation. The average diameter and average volume of the tumors were approximately 10 mm and 500 mm^3, respectively.

Biodistribution

^{18}F-FBB (370 kBq) was injected intravenously into FM3A-implanted mice (n = 4–5); the mice were sacrificed at 0.5, 1, 3, and 6 h after the injection. For the pretargeting

study, we used the protocol that has been previously reported as an optimal method [13]. The mice (n = 4–5) were intravenously injected with 30 μg of POS; after 24 h, ^{18}F-FBB (370 kBq) was injected intravenously. The mice were sacrificed at the same time points as mentioned above. Whole organs were immediately obtained and weighed, and their radioactivity was measured. The results were expressed in terms of the percent injected dose per gram of tissue (%ID/g).

In vivo blocking study

FM3A-implanted mice (n = 4) were pretargeted with POS (30 μg); after 23.5 h, the mice were injected with a vehicle or saline solution of D-biotin (1 nmol). After another 30 min, ^{18}F-FBB (370 kBq) was administered and 3 h later, the mice were sacrificed. Whole organs were immediately removed and weighed, and their radioactivity was measured. The results were expressed as %ID/g.

^{18}F-FBB accumulation vs. HIF-1 transcriptional activity in tumors in mice pretargeted with POS

Some Suit2/Luc-implanted mice (n = 8) were pretargeted with 30 μg of POS. After 24 h, ^{18}F-FBB (370 kBq for 5 mice and 18.5 MBq for 3 mice) was administered intravenously. For immunohistochemical analysis, the mice that received the higher dose of ^{18}F-FBB were intraperitoneally injected with pimonidazole (PIMO, 60 mg/kg) 1 h after the ^{18}F-FBB

injection. Further 2.5 h after the ^{18}F-FBB injection, 200 μL D-luciferin solution (10 mg/mL in PBS; VivoGlo Luciferin, Promega, WI) was injected intraperitoneally. After 20 min, the mice were anesthetized with 2.5% isoflurane, and bioluminescence imaging was performed using IVIS Spectrum System (Xenogen, Alameda, CA). The signal intensity within the tumors was analyzed using Living Image 3.0 software (Xenogen). The mice were sacrificed 3 h after the ^{18}F-FBB injection, the radioactivity of the tumors was measured, and the results were expressed in terms of %ID. The tumor specimens obtained from the mice injected with the higher dose of ^{18}F-FBB were subjected to an autoradiographic study.

Another set of Suit2/Luc-implanted mice (n = 4) were pretargeted with 30 μg of POS. After 24 h, ^{18}F-FBB (18.5 MBq) was administered intravenously and 6 h later, the bioluminescence signal and radioactivity were compared using the procedure described above. After the radioactivity measurement, the tumor specimens were subjected to metabolite analysis.

Size-exclusion analysis of radioactivity in tumors

After bioluminescence imaging, each mouse was anesthetized with 2.5% isoflurane, and urine was collected from its bladder. The mice were then sacrificed, and their tumors were immediately removed. Extracts were prepared using a previously reported method [13], with a slight modification. In brief, the tumors were homogenized in ice-cold 0.1 M Tris-HCl buffer containing 1% sodium dodecylsulfate and 0.15 M NaC1 (pH 6.5), by using a Polytron

homogenizer (PT10-35; Kinematica AG, Switzerland). The preparations were then centrifuged at 4°C and 4,600 × *g* for 20 min. The supernatants and urine were analyzed by size-exclusion chromatography with a PD-10 column.

Autoradiography

Autoradiographic studies were performed on the same mice used for the bioluminescence imaging (n = 3). Ten μm-thick frozen tumor sections were prepared according to a previously reported procedure [21]. The sections were exposed to imaging plates (BAS-SR; Fuji Photo Film Co., Ltd., Tokyo, Japan) for 3 h, and autoradiograms were then obtained and analyzed as previously described [21], except that BAS5000 was used instead of BAS3000 (both scanners, Fuji Photo Film Co., Ltd.).

Immunohistochemical analysis

The adjacent 10 μm-thick sections used in the autoradiographic study were subjected to dual fluorescent immunostaining for HIF-1α and PIMO according to a previously described method [13]. In brief, the sections were fixed, blocked, and treated with anti-human/mouse HIF-1α polyclonal antibody (R&D Systems, Minneapolis, MN), as a primary antibody. The specific signals were detected using an Alexa Fluor 568-conjugated $F(ab')_2$ fragment of goat anti-rabbit antibody (Invitrogen, San Diego, CA). Thereafter, the sections were washed with PBS and treated with fluorescein isothiocyanate

(FITC)-conjugated mouse IgG_1 monoclonal antibody (Chemicon, Temecula, CA) according to the manufacturer's protocol for PIMO staining. The sections were then dried and coverslipped using an antifade reagent (ProLong Gold with DAPI; Invitrogen). Another adjacent section was stained with hematoxylin–eosin (HE). Fluorescent and bright-field microscopic images were obtained using BIOREVO BZ-9000 (Keyence Corp., Osaka, Japan).

PET imaging

^{18}F-FBB (22.2 ± 6.7 MBq) was injected into the tail veins of FM3A-implanted mice (n = 6) 24 h after they were pretargeted with POS (30 μg). The mice were anesthetized with 2.5% isoflurane and placed on a scanner bed in the prone position. At 3 h after the injection, the mice were imaged for 15 min by using eXplore VISTA (GE Healthcare Bioscience). An energy window of 250–700 keV was used. Before reconstruction, the raw data were corrected for random and scattered coincidences, and radioactive decay. Attenuation correction was not performed. PET images were reconstructed according to a standard filtered back-projection procedure (FBP) with a Ramp filter (alpha, 1.0; cutoff, 1.0) or by using a two-dimensional ordered-subset expectation maximization algorithm (2D-OSEM; iterations, 2; subsets, 16). The regions of interest (ROIs) were drawn on the tumor and the corresponding area in the left thigh of the FBP-reconstructed images.

Statistical analyses

The two groups were compared using the Mann–Whitney *U* test, and correlation coefficients were assessed using the Spearman rank analysis. Values of $P < 0.05$ were considered statistically significant.

Results

Radiosynthesis of ^{18}F-FBB

The decay-uncorrected radiochemical yield from ^{18}F-SFB as a starting material was 38%; radiochemical purity, >95%; total synthesis time, 70–100 min; and specific activity at the end of synthesis, >97 GBq/μmol (limit of detection).

Binding of POS and ^{18}F-FBB

After the incubation of ^{18}F-FBB with POS, the radioactivity was detected at macromolecular fraction, as determined using size-exclusion chromatography; this indicated that ^{18}F-FBB bound to POS (data not shown). The binding of ^{18}F-FBB to POS was not inhibited by D-biotin at concentrations <100 nM (binding rate, 99.7% ± 0.2%), whereas it was completely inhibited by 1000 nM D-biotin (binding rate, 6.0% ± 1.3%); the results of inhibition study are similar to those using ^{18}F-FBB alone (5.5% ± 0.5%), i.e., in the case of non-specific absorption to the column (Fig. 2).

Biodistribution

An examination of the biodistribution of ^{18}F-FBB alone revealed that both the tumor-to-blood and the tumor-to-muscle ratios were less than 1 at all time points. This indicated that ^{18}F-FBB did not accumulate in the tumors. Moreover, ^{18}F-FBB was rapidly cleared from all organs, except the intestine (Table 1). In contrast, in the pretargeted group, tumor accumulation of ^{18}F-FBB 3 h after injection was 2.85% ± 0.55% ID/g, which was more than 20-fold than for ^{18}F-FBB alone (0.11% ± 0.10% ID/g) (Table 2). The tumor-to-blood and tumor-to-muscle ratios were greater than 1 as early as 30 min after the injection, and both these ratios increased in a time-dependent manner because of the rapid clearance of ^{18}F-FBB from the body. Although ^{18}F-FBB accumulation in the kidneys and intestine was high, the radioactivity in the other normal tissues showed a more rapid decrease than in the tumor (Table 2). Pretreatment with D-biotin markedly decreased ^{18}F-FBB accumulation (80%) in the tumors (Table 3). The ^{18}F-FBB accumulation in the other tissues also decreased following treatment with D-biotin.

^{18}F-FBB accumulation vs. HIF-1 transcriptional activity in tumors in mice pretargeted with POS

A significant positive correlation was observed between HIF-1-induced luciferase bioluminescence and ^{18}F-FBB accumulation 3 h after injection in tumors in mice pretargeted

with POS ($R = 0.72$, $P < 0.05$; Fig. 3). A similar correlation was also observed at 6 h after the injection ($R = 0.70$, $P < 0.05$, data not shown).

Size-exclusion analysis of radioactivity in tumors

The recovery of radioactivity from the tumor samples was 94% ± 7.4%, and that from the PD-10 columns was 98% ± 14%. A major proportion of the radioactivity was eluted in a macromolecular fraction (79% ± 5.8%, $n = 4$).

Urine analysis was performed using 2 samples, because the quantity of urine obtained from 2 mice was too small. In the case of the urine samples, the recovery of radioactivity from the PD-10 columns was 92% and 99%. More than 99% of the radioactivity of both samples was eluted in a small-molecule fraction.

PET imaging

The high-resolution PET imaging of the mice clearly showed the tumors implanted in the right thigh (Fig. 4). The calculated tumor-to-muscle ratio was 3.4 ± 1.4.

Histology, autoradiography, and immunohistochemistry

HE staining revealed the presence of necrotic areas in the tumor (Fig. 5A). PIMO-positive areas were located in the center of the section, surrounding the necrotic core (Fig. 5B), whereas HIF-1α-positive areas were present peripherally (Fig. 5C). The

autoradiogram showed that the distribution of ^{18}F-FBB in the POS-pretargeted tumor was heterogeneous (Fig. 5D). Most of the ^{18}F-FBB-accumulated areas corresponded to the HIF-1α-positive areas. These findings were similar for each tumor examined in this study.

Discussion

The most important aspect of the present study was to evaluate whether the accumulation of ^{18}F-FBB in POS-pretargeted tumors reflects the level of HIF-1 expression or activity. For this purpose, we compared ^{18}F-FBB accumulation with HIF-1 transcriptional activity and HIF-1 immunohistochemical signal among tumors in the same animals that expressed the HIF-1-dependent luciferase reporter gene. In the tumors in the mice pretargeted with POS, the accumulated radioactivity at both 3 and 6 h after the administration of ^{18}F-FBB significantly correlated with the luciferase bioluminescence, i.e., the HIF-1 activity. Furthermore, the tumor-to-blood ratios at 3 and 6 h were also similar. On the basis of these results, we performed the PET-imaging study at 3 h after the injection of ^{18}F-FBB, because imaging in the early phase after probe injection is preferred in order to avoid radioactive decay and to reduce radiation exposure. The PET images showed the heterogeneous intratumoral distribution of ^{18}F-FBB in the mice pretargeted with POS; this result would reflect the HIF-1-active regions because the intratumoral HIF-1-active regions have been reported to be heterogeneous [22]. In fact, the majority of ^{18}F-FBB-accumulated areas

corresponded to the HIF-1α-positive areas observed on autoradiography. Therefore, these findings indicate that PET imaging with POS pretargeting and the use of ^{18}F-FBB can help detect intratumoral HIF-1-active regions. These findings are in accordance with those of our previous study where ^{123}I-IBB was used instead of ^{18}F-FBB [13]. Because the lipophilicity of ^{18}F-FBB is lower than that of ^{123}I-IBB, ^{18}F-FBB showed faster blood clearance and a higher tumor-to-blood ratio within a short duration after the injection.

Some hypoxia-imaging probes—such as ^{18}F-fluoromisonidazole (^{18}F-FMISO), 1-α-D-(5-deoxy-5-^{18}F-fluoroarabinofuranosyl)-2-nitroimidazole (^{18}F-FAZA), and ^{64}Cu-diacetyl-bis(N^4-methylthiosemicarbazone) (^{64}Cu-ATSM)—have been developed [23, 24]. These probes can detect low oxygen pressures (less than 10 mmHg), and are useful in predicting the efficacy of radiotherapy [25]. In the present study, the distribution pattern of ^{18}F-FBB in the POS-pretargeted tumor was different from that in the PIMO-positive areas. This result is somewhat different from that obtained in our previous studies where ^{125}I-IBB, which was used in the pretargeting study, and ^{125}I-IPOS were mainly distributed near the PIMO-positive areas [12, 13]. One reason for this discordant result may be the difference in the tumor models used. Suit2 pancreatic tumor cells were used for the autoradiographic and histological analyses in the present study, whereas MDA-MB-231 mammary tumor cells were used in the case of the ^{125}I-IPOS study [12]. Another reason could be the difference in tumor size. The tumor volume used in the present study was approximately 1.5 times greater than that used in the ^{125}I-IBB study [13]. In fact, even with the same tumor model, similarity

between the distribution patterns of HIF-1α- and PIMO-positive areas depended on the tumor size; these areas were adjacently located in small tumors but had a different distribution pattern in large tumors [26]. Oh et al. reported that ^{64}Cu-ATSM accumulated on the surface of the tumor, whereas PIMO-positive areas located in the center [27]. This finding is similar to that obtained in the present study on ^{18}F-FBB distribution patterns in POS-pretargeted tumors; however the researchers have not determined HIF-1α expression in the tumor model used in their study. A direct comparison between the POS/^{18}F-FBB system and other hypoxia imaging probes will help clarifying the differences in the characteristics of the tumor cells existed in each area where probe accumulation was observed, and in the information obtained from each image.

The basic requirements of an effective biotin derivative for the pretargeting approach include stability against metabolism *in vivo*, rapid clearance from the circulation, and a binding affinity to (strept)avidin. The first-generation radiolabeled biotin derivatives were easily degraded by biotinidase [28]. Biotinidase-mediated degradation can be stopped by creating a reversed amide bond (i.e., NH−CO bond) between the valeryl chain of biotin and the prosthetic group [29]. On the basis of these reports, we decided to convert the terminal carboxylic group of biotin into a primary amine. We found that ^{18}F-FBB stably existed in mouse plasma (data shown in the supplemental materials), indicating that this compound was resistant to degradation by biotinidase. The results of the biodistribution study revealed that the accumulated radioactivity in the bone was low and that it did not increase in a

time-dependent manner. These results suggest that ^{18}F-FBB is resistant to defluorination *in vivo*. Furthermore, ^{18}F-FBB was rapidly cleared from the blood. ^{18}F-FBB bound to POS and the binding was inhibited by D-biotin both *in vitro* and *in vivo*. These results indicate that ^{18}F-FBB meets the basic requirements of an effective biotin derivative for use in the pretargeting approach.

We found that ^{18}F-FBB accumulated in the POS-pretargeted tumors. Further, this accumulation was inhibited by D-biotin and a major proportion of the radioactivity of the tumor was attributable to macromolecules. Taken together, these results indicate that the intratumoral radioactivity was caused by the binding of ^{18}F-FBB to the SAV moiety of POS. Thus, we concluded that ^{18}F-FBB can bind streptavidin not only *in vitro* but also *in vivo*. The amount of ^{18}F-FBB accumulation in the tumor was not as high as that of ^{18}F-FDG [30]; this finding could have been due to the limited expression of HIF-1. The expression of HIF-1 is not ubiquitous, but heterogeneous, and is small in tumors [31]. In fact, radioligand accumulation in tumors harboring HIF-1-dependent reporter genes has been reported to range from 1% to 2% ID/g in previous studies [31-33]. Furthermore, the amount of ^{18}F-FBB accumulation was similar to that of other hypoxia-imaging probes such as ^{18}F-FMISO and ^{64}Cu-ATSM (2–5% ID/g) [30, 34, 35].

In the pretargeted group, some abdominal organs showed higher radioactivity accumulation than the tumor. The high background activity in the abdominal region hampers the evaluation of the HIF-1 activity in the abdomen and pelvis, and further modification is

required for such an evaluation. The radioactivity of the liver and kidneys may be attributable to the high accumulation of POS in these tissues [12]. Pretreatment of D-biotin decreased ^{18}F-FBB accumulation in the liver and kidneys, suggesting that not all the POS in these tissues was degraded or cleared within 24 h. The slow rate of degradation is a drawback of using POS. Optimization of the interval between the POS and ^{18}F-FBB administration is necessary when imaging HIF-1-active regions in the liver and kidneys. On the other hand, the radioactivity in the intestine was not blocked by D-biotin pretreatment. It is reported that biotinidase, which is involved in the transport of biotin, exists in the intestine [36]. Thus, radioactivity accumulation in the intestine would reflect the behavior of ^{18}F-FBB itself, and not its binding to POS. In this case, the biotin derivatives that show faster clearance from the body [37] may be effective agents.

Conclusion

We have developed a novel radiolabeled biotin derivative, ^{18}F-FBB, and confirmed its ability to bind to the streptavidin moiety both *in vitro* and *in vivo*. ^{18}F-FBB accumulated in the tumors pretargeted with POS; these tumors were clearly visualized on PET imaging. The accumulation of ^{18}F-FBB significantly correlated with the HIF-1 transcriptional activity, and the intratumoral distribution of ^{18}F-FBB corresponded to HIF-1α-positive areas in the tumors pretargeted with POS. These findings suggest that POS and ^{18}F-FBB are potent probes for the

PET imaging of HIF-1-active areas in tumors.

Acknowledgments

We are grateful to Hiroyuki Kimura, Kenji Tomatsu, and Yu Ogawa for preparation of ^{18}F-SFB, and Kei Ogawa for skilled technical assistance.

This study was supported in part by Health Labour Sciences Research Grant for Research on Advanced Medical Technology from the Ministry of Health, Labour and Welfare of Japan; “R&D of Molecular Imaging Equipment for Malignant Tumor Therapy Support” by the New Energy and Industrial Technology Development Organization (NEDO), Japan; and a Grant-in-Aid for Exploratory Research (17659010) and a Grant-in-Aid for Young Scientists (B) (21791187) from the Ministry of Education, Culture, Sports, Science and Technology of Japan.

Conflict of interest

The authors have no conflict of interest.

References

1. Vaupel P, Kallinowski F, Okunieff P (1989) Blood flow, oxygen and nutrient supply, and metabolic microenvironment of human tumors: a review. Cancer Res 49:6449-6465

2. Brown JM (2000) Exploiting the hypoxic cancer cell: mechanisms and therapeutic strategies. Mol Med Today 6:157-162

3. Hockel M, Vaupel P (2001) Tumor hypoxia: definitions and current clinical, biologic, and molecular aspects. J Natl Cancer Inst 93:266-276

4. Semenza GL (2007) Life with oxygen. Science 318:62-64

5. Semenza GL (2003) Targeting HIF-1 for cancer therapy. Nat Rev Cancer 3:721-732

6. Dewhirst MW, Cao Y, Moeller B (2008) Cycling hypoxia and free radicals regulate angiogenesis and radiotherapy response. Nat Rev Cancer 8:425-437

7. Wang GL, Jiang BH, Rue EA, Semenza GL (1995) Hypoxia-inducible factor 1 is a basic-helix-loop-helix-PAS heterodimer regulated by cellular O_2 tension. Proc Natl Acad Sci U S A 92:5510-5514

8. Harada H, Kizaka-Kondoh S, Li G et al (2007) Significance of HIF-1-active cells in angiogenesis and radioresistance. Oncogene 26:7508-7516

9. Harada H, Kizaka-Kondoh S, Hiraoka M (2005) Optical imaging of tumor hypoxia and evaluation of efficacy of a hypoxia-targeting drug in living animals. Mol Imaging 4:182-193

10. Kizaka-Kondoh S, Konse-Nagasawa H (2009) Significance of nitroimidazole compounds and hypoxia-inducible factor-1 for imaging tumor hypoxia. Cancer Sci 100:1366-1373

11. Kizaka-Kondoh S, Tanaka S, Harada H, Hiraoka M (2009) The HIF-1-active microenvironment: an environmental target for cancer therapy. Adv Drug Deliv Rev 61:623-632

12. Kudo T, Ueda M, Kuge Y et al (2009) Imaging of HIF-1-active tumor hypoxia using a protein effectively delivered to and specifically stabilized in HIF-1-active tumor cells. J Nucl Med 50:942-949

13. Ueda M, Kudo T, Kuge Y et al (2010) Rapid detection of hypoxia-inducible factor-1-active tumours: pretargeted imaging with a protein degrading in a mechanism similar to hypoxia-inducible factor-1α. Eur J Nucl Med Mol Imaging [in press]

14. Shoup TM, Fischman AJ, Jaywook S, Babich JW, Strauss HW, Elmaleh DR (1994) Synthesis of fluorine-18-labeled biotin derivatives: biodistribution and infection localization. J Nucl Med 35:1685-1690

15. Vaidyanathan G, Zalutsky MR (2006) Synthesis of N-succinimidyl 4-[^{18}F]fluorobenzoate, an agent for labeling proteins and peptides with ^{18}F. Nat Protoc 1:1655-1661

16. Hara T, Higashi T, Nakamoto Y et al (2009) Significance of chronic marked

hyperglycemia on FDG-PET: is it really problematic for clinical oncologic imaging? Ann Nucl Med 23:657-669

17. Ono M, Watanabe R, Kawashima H et al (2009) Fluoro-pegylated chalcones as positron emission tomography probes for in vivo imaging of beta-amyloid plaques in Alzheimer's disease. J Med Chem 52:6394-6401

18. Kimura H, Tomatsu K, Kawashima H et al (2009) Development of one-flow synthesis method for N-succinimidyl 4-[F-18]fluorobenzoate ([F-18]SFB) using microreactor for 3-step-reaction. J Label Compd Radiopharm 52:S9-S9

19. Tang G, Zeng WB, Yu MX, Kabalka G (2008) Facile synthesis of N-succinimidyl 4-[F-18]fluorobenzoate ([F-18]SFB) for protein labeling. J Label Compd Radiopharm 51:68-71

20. Kizaka-Kondoh S, Itasaka S, Zeng L et al (2009) Selective killing of hypoxia-inducible factor-1-active cells improves survival in a mouse model of invasive and metastatic pancreatic cancer. Clin Cancer Res 15:3433-3441

21. Ueda M, Iida Y, Tominaga A et al (2010) Nicotinic acetylcholine receptors expressed in the ventralposterolateral thalamic nucleus play an important role in anti-allodynic effects. Br J Pharmacol 159:1201-1210

22. Picchio M, Beck R, Haubner R et al (2008) Intratumoral spatial distribution of hypoxia and angiogenesis assessed by ^{18}F-FAZA and ^{125}I-Gluco-RGD autoradiography. J Nucl Med 49:597-605

23. Krohn KA, Link JM, Mason RP (2008) Molecular imaging of hypoxia. J Nucl Med 49 Suppl 2:129S-148S

24. Mees G, Dierckx R, Vangestel C, Van de Wiele C (2009) Molecular imaging of hypoxia with radiolabelled agents. Eur J Nucl Med Mol Imaging 36:1674-1686

25. Dunphy MP, Lewis JS (2009) Radiopharmaceuticals in preclinical and clinical development for monitoring of therapy with PET. J Nucl Med 50 Suppl 1:106S-121S

26. Lehmann S, Stiehl DP, Honer M et al (2009) Longitudinal and multimodal in vivo imaging of tumor hypoxia and its downstream molecular events. Proc Natl Acad Sci U S A 106:14004-14009

27. Oh M, Tanaka T, Kobayashi M et al (2009) Radio-copper-labeled Cu-ATSM: an indicator of quiescent but clonogenic cells under mild hypoxia in a Lewis lung carcinoma model. Nucl Med Biol 36:419-426

28. Chauhan J, Dakshinamurti K (1986) Purification and characterization of human serum biotinidase. J Biol Chem 261:4268-4275

29. Foulon CF, Alston KL, Zalutsky MR (1997) Synthesis and preliminary biological evaluation of (3-iodobenzoyl)norbiotinamide and ((5-iodo-3-pyridinyl)carbonyl)norbiotinamide: two radioiodinated biotin conjugates with improved stability. Bioconjug Chem 8:179-186

30. Liu RS, Chou TK, Chang CH et al (2009) Biodistribution, pharmacokinetics and PET imaging of [^{18}F]FMISO, [^{18}F]FDG and [^{18}F]FAc in a sarcoma- and

inflammation-bearing mouse model. Nucl Med Biol 36:305-312

31. Serganova I, Doubrovin M, Vider J et al (2004) Molecular imaging of temporal dynamics and spatial heterogeneity of hypoxia-inducible factor-1 signal transduction activity in tumors in living mice. Cancer Res 64:6101-6108

32. Hsieh CH, Kuo JW, Lee YJ, Chang CW, Gelovani JG, Liu RS (2009) Construction of mutant TKGFP for real-time imaging of temporal dynamics of HIF-1 signal transduction activity mediated by hypoxia and reoxygenation in tumors in living mice. J Nucl Med 50:2049-2057

33. Wen B, Burgman P, Zanzonico P et al (2004) A preclinical model for noninvasive imaging of hypoxia-induced gene expression; comparison with an exogenous marker of tumor hypoxia. Eur J Nucl Med Mol Imaging 31:1530-1538

34. Lewis JS, McCarthy DW, McCarthy TJ, Fujibayashi Y, Welch MJ (1999) Evaluation of ^{64}Cu-ATSM in vitro and in vivo in a hypoxic tumor model. J Nucl Med 40:177-183

35. Piert M, Machulla HJ, Picchio M et al (2005) Hypoxia-specific tumor imaging with ^{18}F-fluoroazomycin arabinoside. J Nucl Med 46:106-113

36. Dakshinamurti K, Chauhan J, Ebrahim H (1987) Intestinal absorption of biotin and biocytin in the rat. Biosci Rep 7:667-673

37. Hainsworth J, Harrison P, Mather SJ (2005) Preparation and characterization of a DOTA-lysine-biotin conjugate as an effector molecule for pretargeted radionuclide

therapy. Bioconjug Chem 16:1468-1474

Tables

Table 1. Biodistribution of ^{18}F-FBB in FM3A-implanted mice.

	Time after injection (h)			
Organ	0.5	1	3	6
Blood	1.68 ± 0.19	0.86 ± 0.12	0.10 ± 0.07	0.04 ± 0.01
Liver	12.07 ± 1.11	7.30 ± 1.24	0.44 ± 0.06	0.24 ± 0.11
Kidney	10.19 ± 1.14	6.42 ± 0.75	0.42 ± 0.07	0.24 ± 0.12
Intestine	17.99 ± 1.92	21.12 ± 7.27	7.72 ± 1.15	3.72 ± 1.81
Tumor	1.38 ± 0.60	0.77 ± 0.29	0.11 ± 0.10	0.05 ± 0.03
Muscle	2.08 ± 0.23	1.70 ± 0.74	0.09 ± 0.06	0.13 ± 0.08
Bone	1.14 ± 0.96	1.54 ± 0.52	0.27 ± 0.20	0.20 ± 0.17
Tumor/Blood	0.83 ± 0.39	0.90 ± 0.30	0.64 ± 0.20	0.94 ± 0.30
Tumor/Muscle	0.66 ± 0.26	0.66 ± 0.71	0.95 ± 0.61	0.36 ± 0.37

Organ uptake values are expressed as the percent injected dose per gram of tissue, except in the case of the tumor/blood and tumor/muscle ratios. Values are represented as the mean ± SD. n = 4–5

Table 2. Biodistribution of ^{18}F-FBB in FM3A-implanted mice pretargeted with POS.

	Time after injection (h)			
Organ	0.5	1	3	6
Blood	2.79 ± 0.57	1.54 ± 0.47	0.56 ± 0.16	0.57 ± 0.22
Liver	15.02 ± 2.05	12.69 ± 1.86	5.74 ± 1.18	3.76 ± 0.51
Kidney	21.59 ± 3.24	19.52 ± 2.71	9.22 ± 1.92	4.87 ± 0.99
Intestine	12.68 ± 2.60	13.68 ± 2.52	5.95 ± 1.57	1.64 ± 0.51
Tumor	4.65 ± 0.49	4.70 ± 0.97	2.85 ± 0.55	2.48 ± 0.49
Muscle	2.49 ± 0.71	2.55 ± 1.21	0.93 ± 0.40	0.29 ± 0.15
Bone	2.82 ± 0.26	3.92 ± 2.42	1.27 ± 0.42	0.91 ± 0.22
Tumor/Blood	1.73 ± 0.47	3.16 ± 0.59	5.36 ± 1.32	4.91 ± 2.04
Tumor/Muscle	1.98 ± 0.54	2.18 ± 0.75	3.93 ± 2.50	9.51 ± 3.31

Organ uptake values are expressed as the percent injected dose per gram of tissue, except in the case of the tumor/blood and tumor/muscle ratios. Values are represented as the mean ± SD. n = 4–5

Table 3. Blocking study of the biodistribution of ^{18}F-FBB in FM3A-implanted mice pretargeted with POS.

Organ	Vehicle	D-biotin pretreatment
Blood	0.66 ± 0.06	0.22 ± 0.10*
Liver	3.58 ± 1.00	1.48 ± 0.67*
Kidney	3.39 ± 1.05	0.80 ± 0.41*
Intestine	6.59 ± 2.76	7.90 ± 0.98
Tumor	2.06 ± 0.29	0.34 ± 0.14*
Muscle	0.28 ± 0.04	0.14 ± 0.06*
Bone	1.50 ± 1.37	1.31 ± 0.38
Tumor/Blood	4.00 ± 2.38	1.63 ± 0.19*
Tumor/Muscle	7.29 ± 0.94	2.53 ± 1.19**

Organ uptake values are expressed as the percent injected dose per gram of tissue, except in the case of the tumor/blood and tumor/muscle ratios. Values are represented as the mean ± SD. $n = 4$; *$P < 0.05$, **$P < 0.01$ vs. vehicle group.

Fig. 1

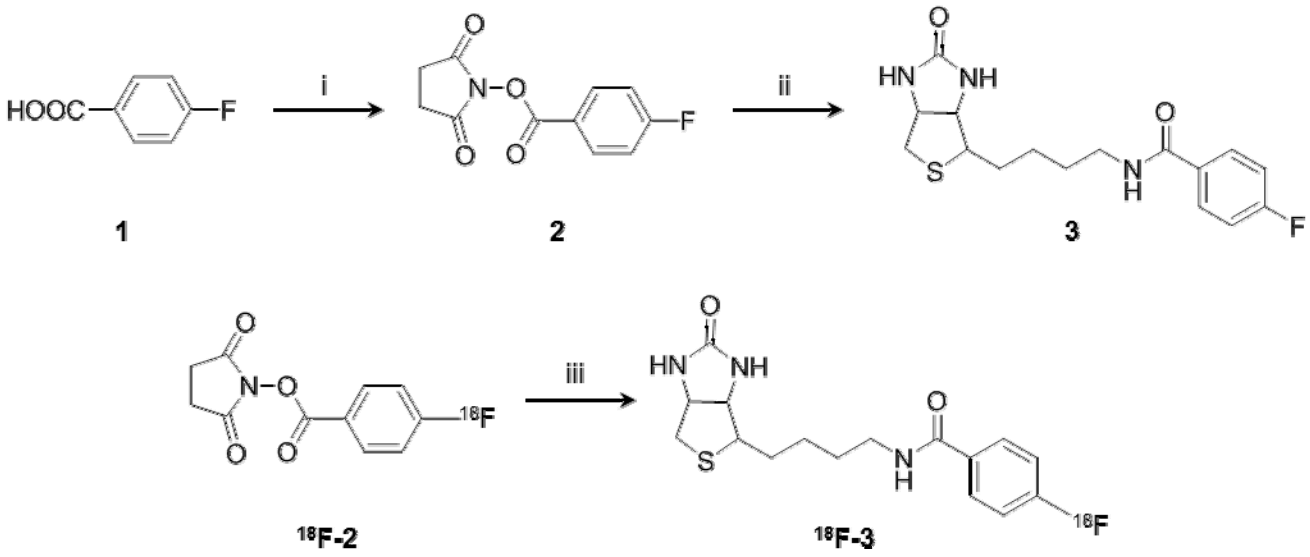

Synthesis of FBB (**3**) and ^{18}F-FBB (^{18}F-**3**). (i) *N*,*N*,*N*′,*N*′-Tetramethyl-*O*-(*N*-succinimidyl)uranium tetrafluoroborate, CH_3CN, 90°C, 10 h. (ii) Norbiotinamine, NEt_3, DMF:H_2O (4:1), r.t., 5 h. (iii) Norbiotinamine, NEt_3, DMF:H_2O (4:1), r.t., 1 h.

Fig. 2

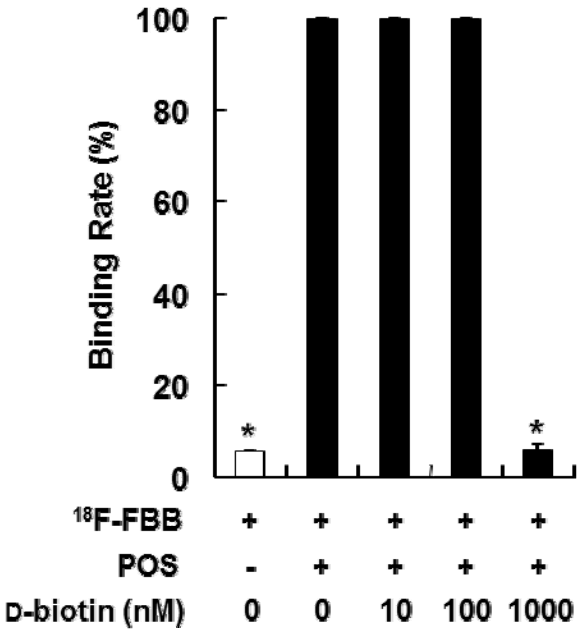

Binding of ^{18}F-FBB to POS. The black columns represent the mean calculated binding rate of ^{18}F-FBB and POS in the presence of various concentrations of D-biotin. The white column represents the calculated binding rate of ^{18}F-FBB alone, which indicates non-specific absorption to the column. D-biotin (1000 nM) significantly inhibited ^{18}F-FBB binding to POS compared to the binding in the other D-biotin-treated group (*$P < 0.05$).

Fig. 3

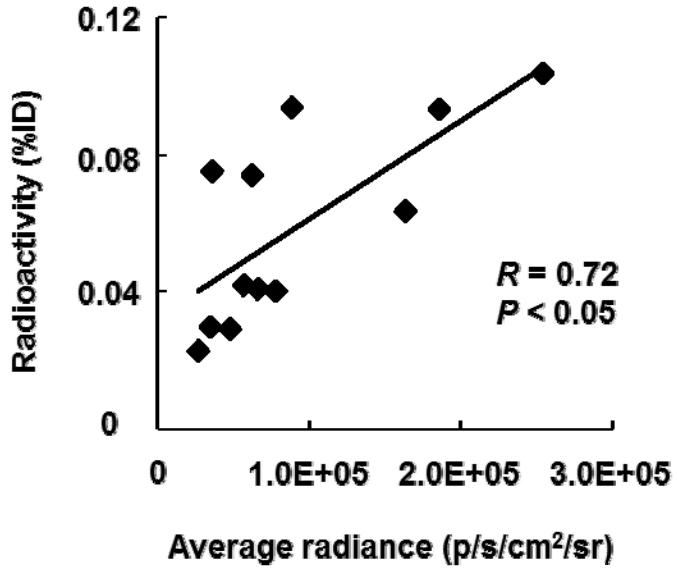

Correlation between the ^{18}F-FBB accumulation at 3 h post-injection and HIF-1 activity within a tumor pretargeted with POS. The ordinate represents accumulated radioactivity (%ID), and the abscissa represents HIF-1-induced luciferase bioluminescence. The correlation coefficient (R) was 0.72, indicating a highly significant correlation ($P < 0.05$).

Fig. 4

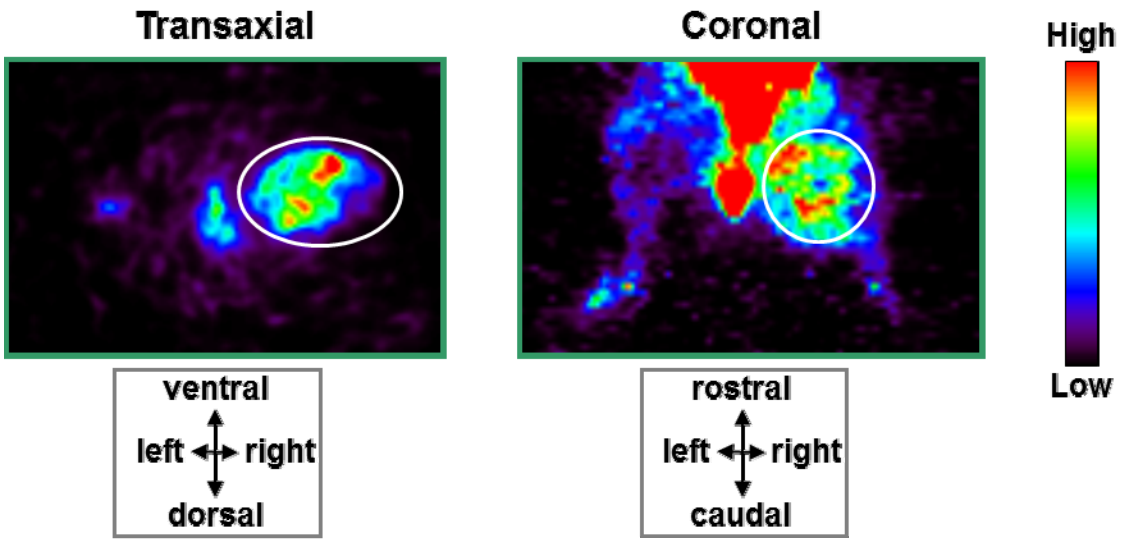

Typical PET images of FM3A-implanted mice. The mice were pretargeted with POS, and 24 h later, they were intravenously injected with ^{18}F-FBB. Images were acquired 3 h after the ^{18}F-FBB injection and reconstructed using 2D-OSEM. Tumors can be clearly visualized in both images (arrow).

Fig. 5

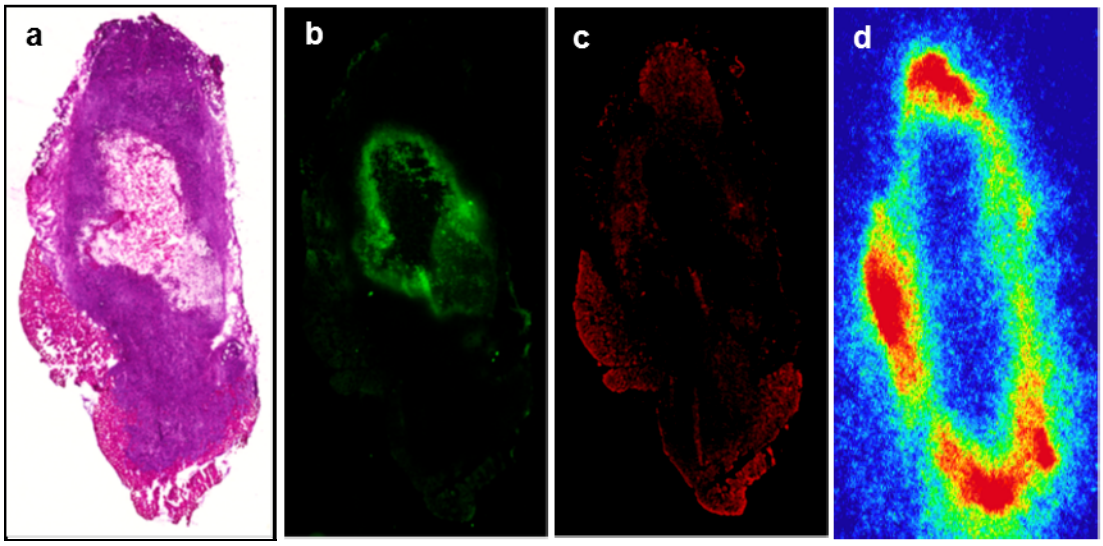

Representative images of HE staining (A), PIMO immunostaining (B), HIF-1α immunostaining (C), and autoradiography (D).